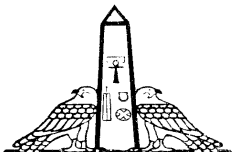

Ain Shams University

Microwave Dielectric Properties of Alkaline Earths Titanate–Lanthanides Titanate Ceramic Bodies

A Thesis Submitted
By

AISHA EZZ EL-DIN REDA GABER MOHAMED

AISHA EZZ EL-DIN REDA GABER MOHAMED
((M. Sc. in Chemistry)

For Fulfillment of the Degree of Ph. D. in Chemistry

Department of Chemistry
Faculty of Science
Ain Shams University
Cairo, Egypt
2013

Microwave Dielectric Properties of Alkaline Earths Titanate–Lanthanides Titanate Ceramic Bodies

A Thesis Submitted

By

AISHA EZZ EL-DIN REDA GABER MOHAMED

(M. Sc. in Chemistry)

For Fulfillment of the Degree of Ph. D. in Chemistry

Supervised by

Prof. Dr. Eglal Rimon Souaya

Professor of Inorganic Chemistry, Department of Chemistry, Faculty of Science, Ain Shams University.

Prof. Dr. Doreya Mohamed Mahmoud Ibrahim

Professor of Chemistry and Technology of Ceramic, Department of Ceramics, Refractories and Building Materials, NRC

Prof. Dr. Doaa Abdel Nabi Abdel Aziz

Professor of Chemistry and Technology of Ceramic, Department of Ceramics, Refractories and Building Materials, NRC

Approval Sheet
P.Sc. Thesis

Entitled

Microwave Dielectric Properties of Alkaline Earths Titanate– Lanthanides Titanate Ceramic Bodies

Thesis Advisors **Thesis Approved**

Prof. Dr. Eglal Rimon Souaya **……...**
Professor of Inorganic Chemistry, Department of Chemistry, Faculty of Science, Ain Shams University.

Prof. Dr. Doreya Mohamed Mahmoud Ibrahim **……...**
Professor of Chemistry and Technology of Ceramic, Department of Refractories, Ceramics and Building Materials, NRC.

Prof. Dr. Doaa Abdel Nabi Abdel Aziz **…….**
Professor of Chemistry and Technology of Ceramic, Department of Refractories, Ceramics and Building Materials, NRC.

Head of Chemistry Department

Prof. Dr. Hesham Ahmed Madian

ACKNOWLEDGMENT

Thanks and indebtedness is directed first and always to ***ALLAH*** for all his graves, without the power he gave me, the accomplishment of his work would have been certainly impossible.

The author feels a deep sense of gratitude to all the people associated in various ways during the progress and completion of this work.

I am cordially indebted to Prof***. Dr. Eglal Rimon Souaya***, (Faculty of Science, Ain Shams University) for her supervision, constructive criticism and deep concern in this work.

My sincere gratefulness to Prof. Dr. ***Doreya Mohamed Mahmoud Ibrahim,*** Prof. of Ceramic Chemistry, Department of Ceramic, NRC, for supervising the research project and fruitful suggestions during this work.

I would like to express my deep gratitude, and sincere thanks to Prof. Dr. ***Doaa Abdel Nabi Abdel Aziz***, Prof. of Ceramic Chemistry, Department of Ceramic, NRC, for suggesting and supervising the research project, helpful discussions and also for the sincere guidance with encouragement during her direct supervision throughout this work.

I am especially indebted to my mother, my father and brothers for their love, sacrifice, and support. They are my first teachers after I came to this world and have set great examples for me about how to live, study, and work.

Abstract

The microwave dielectric properties, the microstructures and the physical properties of (1-x) $A^{2+}TiO_3$- x ($A^{1+}_{0.5}A^{3+}_{0.5}$) TiO_3 ((A^{2+} = Ca), (A^{1+} = Na, Li, K), (A^{3+} = La, Nd)) (x = 0.08, 0.10, 0.20, 0.50and 0.90) but incase potassium (x = 0.02, 0.05, 0.08, 0.10, 0.20, 0.50, 0.90 and 1.0) ceramics are very important candidates for millimeter-wave applications (e.g. filter and antenna). Structural X-ray diffraction analysis confirmed the perovskite structure. The microstructure of the sintered ceramic bodies was analyzed using scanning electron microscopy (SEM) and energy-dispersive X-ray (EDS) microanalysis. The Vector Network Analyzer (VNA) in the frequency range from 50 MHz-13GHz was used to measure the dielectric properties at microwave (MW) frequency range. Several samples with La_2O_3 or Nd_2O_3 were prepared by conventional solid-state route. It was found that the increasing of lanthanides titanates in form of lanthanum or neodymium to $CaTiO_3$ ceramic bodies in most case decreased the sintering temperature by 50^oC at temperature in the range 1100-1350°C. The investigated bodies show a dense microstructure due to the liquid phase development. The results revealed that the microwave dielectric characteristics can be effectively controlled by lanthanides content, secondary phase and microstructure developed. The maximum result of potassium lanthanum content recorded with 10CT-

KLT (x=0.90) and KLT (x=1.0) ceramics sintered at 1300 ^{o}C/2h, was ε_r= 7.8-7.3, respectively, while the same values of high quality factor (Qxf) = 43.33*10^4 at 13 GHz, and low dielectric loss = 0.03*10^{-3} was obtained. According to the microstructure obtained, rod like grains in the KLT body might have enhanced microwave property. Also, the higher values recorded with potassium neodymium oxide were obtained with lower KNT content for 92CT-KNT (x=0.08) ceramic body, sintered at 1300 ^{o}C/2h, where (ε_r) =40, Qxf value (3.33*10^4 at 5 GHz) with lower dielectric loss value (0.13x10^{-3}) may be due to uniform shape which have played an important role for the enhanced microwave property.

CONTENTS

	Page
List of Figures	i
List of Tables	vi
Abstract	viii
Chapter I:	
I. Introduction	1
I.1. Ceramic Materials	1
I.2. Types of Dielectric Materials	2
I.3. Types of Perovskite Dielectric Ceramic Bodies	14
I.4. Characterization of Microwave Dielectric Materials	15
I.5. Types of Microwave Perovskite Ceramic Bodies	24
I.6. Previous Work on the Dielectric Properties of Complex Perovskite ceramics	27
Aim of the work	39
Chapter II:	
II. Materials and Methods	40
I.1. Starting materials	40
II.2. Method of Preparation	40
Chapter III:	
III. Results and Discussion	47

III.I.1. Characterization of (1-x)$CaTiO_3$-x($Li^{1+}_{0.5}La^{3+}_{0.5}$)$TiO_3$(CT-LLT) Samples **47**

1. Phase Composition **47**

2. Densification Parameters **53**

3. Microwave Dielectric Properties **55**

III.I.2. Characterization of (1-x) $CaTiO_3$-x($Na^{1+}_{0.5}La^{3+}_{0.5}$) TiO_3 (CT-NLT) Samples **59**

1. Phase Composition **59**

2. Densification parameters **64**

3. Microwave Dielectric Properties **66**

III.I.3. Characterization of (1-x)$CaTiO_3$-x($K^{1+}_{0.5}La^{3+}_{0.5}$)$TiO_3$ (CT-KLT) Samples **70**

1. Phase Composition **70**

2. Densification parameters **78**

3. Microwave Dielectric Properties **80**

III.I. Conclusion **84**

III.II. Characterization of (1-x)$CaTiO_3$-x($Li^{1+}_{0.5}Nd^{3+}_{0.5}$)$TiO_3$ (CT-LNT) Samples **85**

1. Phase Composition **85**

2. Densification parameters **88**

3. Microwave Dielectric Properties **92**

III.II.2. Characterization of (1-x)$CaTiO_3$-x($Na^{1+}_{0.5}Nd^{3+}_{0.5}$)$TiO_3$ (CT-NNT) Samples **96**

1. Phase Composition **96**

2. Densification parameters **101**

3. Microwave Dielectric Properties **101**

III.II.3. Characterization of (1-x)$CaTiO_3$-x($K^{1+}_{0.5}Nd^{3+}_{0.5}$) TiO_3 (CT-KNT) Samples **105**

1. Phase Composition **106**

2. Densification parameters **114**

3. Microwave Dielectric Properties **114**

III.II. Conclusion **119**

Chapter IV:
Summary and Conclusions **120**

IV.1. Summary **120**

IV.2. Conclusion **126**

References **128**

Arabic summary

LIST OF FIGURES

Fig. No.	List of Figures	Page
Fig. 1:	Sales of Smartphone devices on a global scale by the Telecommunication Agency of the United Nations	3
Fig. 2:	Cubic ABO_3 ($BaTiO_3$) Perovskite Structure	8
Fig. 3:	Crystal structure of $BaTiO_3$, (a) Above the Curie point the cell is cubic (b) Below the Curie point the structure is tetragonal with Ba^{2+} and Ti^{4+} ions displaced relative to O^{2-} ions	9
Fig. 4:	Distorted perovskite of $CaTiO_3$ with orthorhombic symmetry	11
Fig. 5:	Perovskite cubic structure of $CaTiO_3$	12
Fig. 6:	Applications of Microwave Dielectric Ceramics at microwave and mm-wave frequencies.	16
Fig. 7:	Schematic showing a resonant peak and associated parameters.	19
Fig. 8:	Process of shaping of materials used in satellite communication	35
Fig. 9:	Show Schematic resonance peak	46
Fig. 10:	XRD patterns of calcined $(1-x)CaTiO_3$–$x(Li_{0.5}La_{0.5})TiO_3$ powders	48
Fig. 11:	XRD patterns of sintered $(1-x)CaTiO_3$–$x(Li_{0.5}La_{0.5})TiO_3$ ceramic bodies	48
Fig. 12:	Microstructure of $(1-x)CaTiO_3$-$x(Li_{0.5}La_{0.5})TiO_3$ at sintered temperature (a) x=0.08 (92CT-LLT), (b) x=0.10 (90CT-LLT), (c) x=0.20 (80CT-LLT),	51

(d) x=0.50 (50CT-LLT) and (e) x=0.90 (10CT-LLT).

Fig. 13: Physical properties of (1-x)$CaTiO_3$–x($Li_{0.5}La_{0.5}$)TiO_3 bodies as a function of different sintered temperature. 54

Fig. 14: Microwave dielectric properties of (1-x)$CaTiO_3$-x($Li_{0.5}La_{0.5}$)TiO_3 ceramics (a) Dielectric constant (b) Quality factor and Dielectric loss as function of x values. 57

Fig. 15: XRD patterns of calcined (1-x)$CaTiO_3$-x($Na_{0.5}La_{0.5}$)TiO_3 powders 60

Fig. 16: XRD patterns of sintered (1-x)$CaTiO_3$-x($Na_{0.5}La_{0.5}$)TiO_3 ceramic bodies 60

Fig. 17: Microstructure of (1-x)$CaTiO_3$-x($Na_{0.5}La_{0.5}$)TiO_3 at sintered temperature (a) x=0.08 (92CT-NLT), (b) x=0.10 (90CT-NLT), (c) x=0.20 (80CT-NLT), (d)x=0.50 (50CT-NLT) and (e) x=0.90 (10CT-NLT). 63

Fig. 18: Physical properties of (1-x)$CaTiO_3$-x($Na_{0.5}La_{0.5}$)TiO_3 bodies as a function of different sintered temperature**.** 65

Fig. 19: Microwave dielectric properties of (1-x)$CaTiO_3$–x($Na_{0.5}La_{0.5}$)TiO_3 ceramics (a) Dielectric constant (b) Quality factor and Dielectric loss as function of x values. 68

Fig. 20: XRD patterns of calcined (1-x)$CaTiO_3$–x($K_{0.5}La_{0.5}$)TiO_3 powders 71

Fig. 21:	XRD patterns of sintered (1-x)$CaTiO_3$–x$(K_{0.5}La_{0.5})TiO_3$ ceramic bodies	71
Fig. 22:	XRD patterns of calcined (1-x)$CaTiO_3$–x$(K_{0.5}La_{0.5})TiO_3$ powders	72
Fig. 23:	XRD patterns of sintered (1-x)$CaTiO_3$–x$(K_{0.5}La_{0.5})TiO_3$ ceramic bodies	72
Fig. 24:	Microstructure of (1-x)$CaTiO_3$–x$(K_{0.5}La_{0.5})TiO_3$ at sintered temperature (a) x=0.02 (98CT-KLT), (b) x=0.05 (95CT-KLT), (c) x=0.08 (92CT-KLT), (d) x=0.10 (90CT-KLT), (e) x=0.20 (80CT-KLT),(f) x=0.50 (50CT-KLT) and (g) x=0.90 (10CT-KLT) and (h) KLT	75-76
Fig. 25:	Physical properties of (1-x)$CaTiO_3$–x$(K_{0.5}La_{0.5})TiO_3$ bodies at sintered temperature (a) with x =0.02, 0.05 0.08, 0.10 and 0.20 and (b) with x= 0.50, 0.90 and 1.0.	79
Fig. 26:	Microwave dielectric properties of (1-x)$CaTiO_3$-x$(K_{0.5}La_{0.5})TiO_3$ ceramics (a) Dielectric constant (b) Quality factor and Dielectric loss as function of x values.	82
Fig. 27:	XRD patterns of calcined (1-x)$CaTiO_3$-x$(Li_{0.5}Nd_{0.5})TiO_3$ powders	86
Fig. 28:	XRD patterns of sintered (1-x)$CaTiO_3$-x$(Li_{0.5}Nd_{0.5})TiO_3$ ceramic bodies	86
Fig. 29:	Microstructure of (1-x)$CaTiO_3$–x$(Li_{0.5}Nd_{0.5})TiO_3$ at sintered temperature (a)x=0.08 (92CT-NLT), (b)x=0.10 (90CT-NLT), (c)x=0.20 (80CT-NLT), (d)x=0.50(50CT-NLT)and(e)x=0.90(10CT-NLT).	89

Fig. 30: Physical properties of (1-x)$CaTiO_3$-x($Li_{0.5}Nd_{0.5}$)TiO_3 bodies at different sintered temperature. 91

Fig. 31: Microwave dielectric properties of (1-x)$CaTiO_3$-x($Li_{0.5}Nd_{0.5}$)TiO_3 ceramics (a) Dielectric constant (b) Quality factor and Dielectric loss as function of x value 94

Fig. 32: XRD patterns of calcined (1-x)$CaTiO_3$–x($Na_{0.5}Nd_{0.5}$)TiO_3 powders 97

Fig. 33: XRD patterns of sintered (1-x)$CaTiO_3$–x($Na_{0.5}Nd_{0.5}$)TiO_3 ceramic bodies 97

Fig. 34: Microstructure of (1-x)$CaTiO_3$–x($Na_{0.5}Nd_{0.5}$)TiO_3 at sintered temperature (a) x=0.08 (92CT-NLT), (b) x=0.1 (90CT-NLT), (c) x=0.2 (80CT-NLT), (d) x=0.5 (50CT-NLT) and (e) x=0.90 (10CT-NLT). 100

Fig. 35: Physical properties of (1-x)$CaTiO_3$-x($Na_{0.5}$ $Nd_{0.5}$)TiO_3 bodies at different sintered temperature. 103

Fig. 36: Microwave dielectric properties of (1-x)$CaTiO_3$-x($Na_{0.5}Nd_{0.5}$)TiO_3 ceramics (a) Dielectric constant (b) Quality factor and Dielectric loss as function of x value 104

Fig. 37: XRD patterns of calcined (1-x)$CaTiO_3$–x($K_{0.5}Nd_{0.5}$)TiO_3 powders 108

Fig. 38: XRD patterns of sintered (1-x)$CaTiO_3$–x($K_{0.5}Nd_{0.5}$)TiO_3 ceramic bodies 108

Fig. 39: XRD patterns of calcined (1-x)$CaTiO_3$–x($K_{0.5}Nd_{0.5}$)TiO_3 powders 109

Fig. 40: XRD patterns of sintered (1-x)$CaTiO_3$–x($K_{0.5}Nd_{0.5}$)TiO_3 ceramic bodies 109

Fig. 41: Microstructure of (1-x)$CaTiO_3$–x($K_{0.5}Nd_{0.5}$)TiO_3 at sintered temperature (a) x=0.02 (98CT-KNT), (b) x=0.05 (95CT-KNT), (c) x=0.02 (92CT-KNT), (d) x=0.10 (90CT-KNT) and (e) x=0.20 (80CT-KNT), (f) x=0.50 (50CT-KNT) and (g) x=0.90 (10CT-KNT) and (h) KNT 111-112

Fig. 42: Physical properties of (1-x)$CaTiO_3$–x($K_{0.5}Nd_{0.5}$)TiO_3 bodies at sintered temperature (a) with x =0.02, 0.05 0.08, 0.10 and 0.20 and (b) with x= 0.50, 0.90 and 1.0. 116

Fig. 43: Microwave dielectric properties of (1-x)$CaTiO_3$-x($K_{0.5}Nd_{0.5}$)TiO_3 ceramics (a) Dielectric constant (b) Quality factor and Dielectric loss as function of x values. 117

LIST OF TABLES

Table No.	List of Tables	Page
Table 1:	Change in d-spacing (2θ) of peak with $(1-x)CaTiO_3–x(Li_{0.5}La_{0.5})TiO_3$	49
Table 2:	EDS analysis of 50CT-LLT with x=0.50	52
Table 3:	physical and microwave dielectric properties of $(1-x)CaTiO_3–x(Li_{0.5}La_{0.5})TiO_3$ ceramic bodies at different sintered temperature	58
Table 4:	Change in d-spacing (2θ) of peak with $(1-x)CaTiO_3$-$x(Na_{0.5}La_{0.5})TiO_3$	61
Table 5:	physical and microwave dielectric properties of $(1-x)CaTiO_3–x(Na_{0.5}La_{0.5})TiO_3$ ceramic bodies at different sintered temperature	69
Table 6:	Change in d-spacing (2θ) of peak in $(1-x)CaTiO_3–x(K_{0.5}La_{0.5})TiO_3$	73
Table 7:	EDS analysis of 80CT-KLT with x=0.20	77
Table 8:	physical and microwave dielectric properties of $(1-x)CaTiO_3–x(K_{0.5}La_{0.5})TiO_3$ ceramic bodies at different sintered temperature	83
Table 9:	Change in d-spacing (2θ) of peak with $(1-x)CaTiO_3$ -$x(Li_{0.5}Nd_{0.5})TiO_3$	87
Table 10:	EDS analysis of 0.90CT-LLT with x=0.10	90
Table :11	physical and microwave dielectric properties of $(1-x)CaTiO_3–x(Li_{0.5}Nd_{0.5})TiO_3$ ceramic bodies at different sintered temperature	95